Original Article

Institution of MECHANICAL ENGINEERS

Journal of MECHANICAL ENGINEERING SCIENCE

Proc IMechE Part C:
J Mechanical Engineering Science
227(4) 730–743

DOI: 10.1177/0954406212454390
pic.sagepub.com

SAGE

Theoretical flowrate characteristics of the conjugated involute internal gear pump

Hua Zhou and Wei Song

Abstract

The aim of this article is to study the theoretical flowrate characteristics of the conjugated involute internal gear pump. The conjugated involute internal gear pump has a different internal gear, the profile of which is completely conjugated to that of pinion, from the conventional involute internal gear pump. To describe briefly, the former pump is called 'conjugated pump' while the latter pump 'conventional pump'. This structure makes the conjugated pump have smaller volumes of trapped fluid than the conventional pump, which indicates the conjugated pump has a better flowrate performance. Although there have been numerous investigations into gear pumps, none of them have dealt with the conjugated pumps yet. This article presents a systematic study on the theoretical flowrate characteristics of the conjugated pumps. It is expected to obtain some generalized conclusions to guide the design of internal gear pumps. Firstly, a double envelope concept is applied to derive the mathematical models of the conjugated involute internal gear couple. Next, mesh characteristics of the gear couple, which mainly decide the fluid delivery performance of the pumps, are analyzed. Finally, using a control volume approach, the theoretical flowrate characteristics of the pump under different design parameters of gears are investigated. Results show the conjugated pump has a better performance than the conventional one. To design a conjugated pump with good flowrate characteristics, it's feasible to choose a proper shifting coefficient, a larger tooth number of the pinion, a smaller tooth number of the internal gear, a larger pressure angle and a larger fillet radius, under the condition that no tooth interference occurs.

Keywords

Flowrate characteristic, conjugated involute, internal gear pump

Date received: 23 February 2012; accepted: 20 June 2012

Introduction

Gear pumps are the most often employed power-supplying components in hydrostatic systems, allowing low cost, good efficiency and high reliability. Based on structures, gear pumps are classified into two types: external gear pumps and internal gear pumps.[1] Internal gear pumps have less flowrate pulsation than external gear pumps, which makes them operate quietly and attract attention in applications where people concern environmental noise.[2,3]

Involute internal gear pump is the main product type on the market, cross section of which is shown in Figure 1(a). Figure 1(b) presents another kind of internal gear pump, *conjugated involute internal gear pump*. The only difference between them lies in the tooth profile of internal gear. To describe briefly, we call the pump in Figure 1(a) as 'conventional pump' and the one in Figure 1(b) as 'conjugated pump'. It is known that the profile of pinion mainly comprises an involute and a root fillet. In the conjugated pump, the whole profile of internal gear is completely conjugated to that of pinion. While in the conventional pump, there is no curve conjugated to the root fillet in the profile of internal gear. Additionally, its involute is only partly conjugated to that of pinion. Consequently, clearances among meshing teeth are larger in the conventional pump than those in the conjugated pump (Figure 1). These clearances directly decide the volumes of trapped fluid which induces large pressure ripples and high noise levels to hydrostatic systems. Since the conjugated pump has smaller volumes of trapped fluid, it will consequently have better operating performances than the conventional pump.

Investigations into gear pumps have been done for years, most of which concern the flowrate performances of external gear pumps. Manring and Kasaragadda[3] calculated the instantaneous flowrate

State Key Laboratory of Fluid Power Transmission and Control, Zhejiang University, Hangzhou, P. R. China

Corresponding author:
Wei Song, State Key Laboratory of Fluid Power Transmission and Control, Zhejiang University, Hangzhou, P. R. China.
Email: songwei_zju@163.com

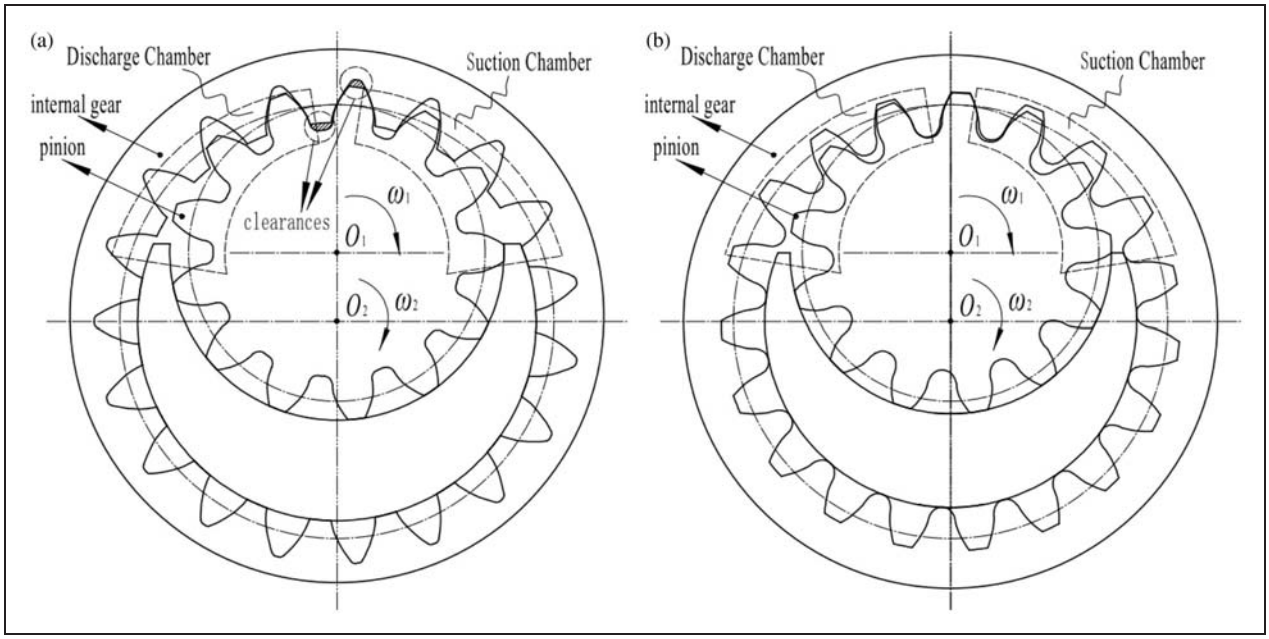

Figure 1. Cross sections of two kinds of internal gear pump: (a) involute internal gear pump; (b) conjugated involute internal gear pump.

of external gear pumps with different tooth numbers for the driving and driven gears and pointed out a bigger tooth number for the driving gear can decrease flowrate pulsation. Casoli and Franzoni[4] presented a numerical model for simulations of external gear pumps. Implemented in AMESim environment, this model shows the fluid dynamics of the pump and allows estimations of flowrate pulsation and volumetric efficiency. Huang and Lian[5] derived a closed flowrate formula of external gear pumps using a control volume approach and indicated parameters including tooth number, pressure angle and addendum coefficient help reduce flowrate pulsation. Using the same approach, Huang et al.[6] obtained a flowrate formula of external helical gear pumps and made a displacement optimization. Results showed the external helical gear pumps with large module, large face width, or small teeth number have great displacements but severe flowrate pulsation. Besides, pressure angle and helical angle affect displacement slightly while large addendum coefficient benefits both displacement and flowrate pulsation.

Compared to external gear pumps, internal gear pumps have fewer investigations, most of which focused on gerotor pumps (or lobe pumps), which are a special type of internal gear pumps and usually applied in low-pressure (below 15 MPa) occasions. Based on the theory of gearing, Colbourne[7] and Beard et al.[8] studied the influences of profile parameters on the flowrate performances of gerotor pumps. Combined simulations and experiments, Gamez-Montero and Codina[9,10] studied the theoretical volumetric characteristics of gerotor pumps, which help understand the dynamic properties of gerotor pumps. Mimimi et al.[11,12] analyzed the theoretical performances of gerotor pumps with different profiles and demonstrated hypotrochoidal profile can be an effective alternative solution for epitrochoidal one. For involute internal gear pumps, Ichikawa[13] calculated the ideal flowrate characteristics by a torque approach. Results showed internal gear pumps have less flowrate pulsation and trapped fluid than external gear pumps. The work of Mimmi and Pennacchi[14] indicates involute internal gear pumps give better performances when the tooth number of pinion is close to that of internal gear.

To the authors' best knowledge, a work dealt with the conjugated pumps is yet to be found and few investigations have systematically studied the flowrate characteristics of internal gear pumps. This article presents a systematic study on the theoretical flowrate characteristics of the conjugated pumps. It is expected to obtain some generalized conclusions to guide the design of internal gear pumps with high performances.

Mathematical models of the conjugated involute internal gear couple

The double envelope concept is frequently used to derive the profiles of gear couples, basic idea of which is developed from the theory of gearing.[15–17] During the derivation, the mathematical model of the pinion is firstly regarded as an envelope to the family of the rack-cutter surfaces. Then, the obtained pinion is assumed as the generating surface and defined as the second envelope to generate internal gear. In this way, the profiles of pinion and internal gear can be easily obtained.

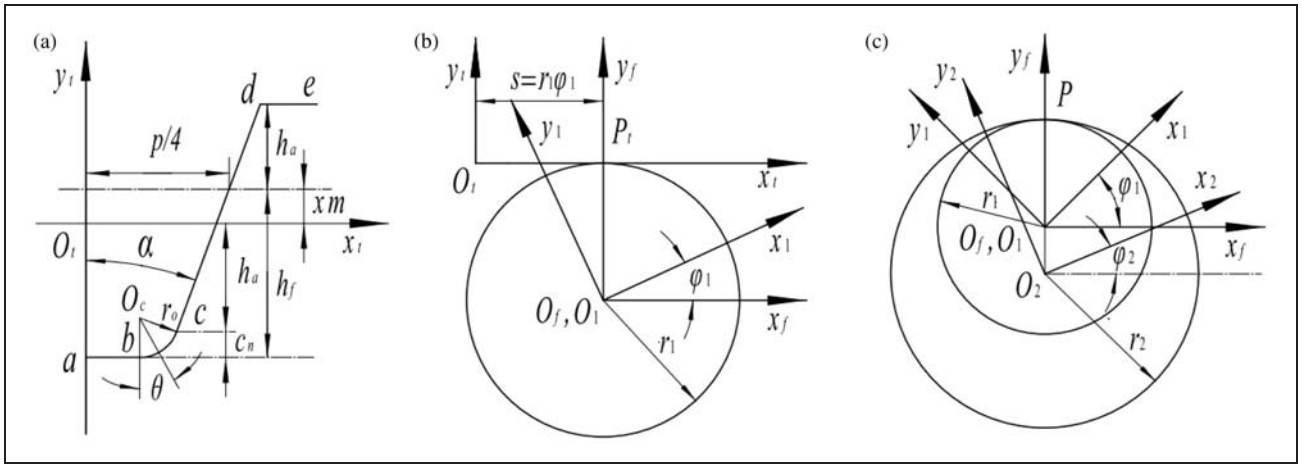

Figure 2. Coordinate systems used in the double envelope process: (a) profile of rack-cutter; (b) generation of pinion; (c) generation of internal gear.

The profile of rack-cutter for involute gears

The involute pinion can be easily generated by a rack-cutter tool. Figure 2(a) shows the profile of rack-cutter for involute gears, including line *ab*, arc *bc*, line *cd* and line *de*. To illustrate the profile, a coordinate system $S_t(O_t, x_t, y_t)$ is built and rigidly connected to the rack-cutter. The x_t axis has a distance of xm from the pitch line of rack-cutter while the y_t axis coinciding with the pitch line of rack-cutter. Here, x is defined as shifting coefficient. Then, the profile can be represented in S_t

$$\boldsymbol{R}_t^{ab} = \begin{bmatrix} x_t^{ab} \\ y_t^{ab} \\ z_t^{ab} \end{bmatrix} = \begin{bmatrix} x_t \\ -h_f + xm \\ 1 \end{bmatrix}, \quad 0 \leqslant x_t \leqslant x_b \tag{1}$$

$$\boldsymbol{R}_t^{bc} = \begin{bmatrix} x_t^{bc} \\ y_t^{bc} \\ z_t^{bc} \end{bmatrix} = \begin{bmatrix} x_t \\ y_{O_c} - \sqrt{r_o^2 - (x_t - x_{O_c})^2} \\ 1 \end{bmatrix}, \quad x_b < x_t \leqslant x_c \tag{2}$$

$$\boldsymbol{R}_t^{cd} = \begin{bmatrix} x_t^{cd} \\ y_t^{cd} \\ z_t^{cd} \end{bmatrix} = \begin{bmatrix} x_t \\ (x_t - \frac{p}{4})\cot a + xm \\ 1 \end{bmatrix}, \quad x_c < x_t \leqslant x_d \tag{3}$$

$$\boldsymbol{R}_t^{de} = \begin{bmatrix} x_t^{de} \\ y_t^{de} \\ z_t^{de} \end{bmatrix} = \begin{bmatrix} x_t \\ h_a + xm \\ 1 \end{bmatrix}, \quad x_d < x_t \leqslant x_e \tag{4}$$

where x_t is the design parameter of rack-cutter. Here, $x_b = x_{Oc} = 0.25\,p - \tan\alpha[h_f - r_o(1 - \sin\alpha)] - r_o\cos\alpha$, $y_{Oc} = -(h_a^* + c_n^*)m + r_o + xm$, $x_c = x_{Oc} + r_o\sin(\pi/2 - \alpha)$, $x_d = p/4 + h_a\tan\alpha$, $x_e = p/2$.

The profile of pinion with involute tooth

To determine the first envelope, the relationship between the rack-cutter and the pinion during the generation is depicted by Figure 2(b). Coordinate systems $S_f(O_f, x_f, y_f)$ and $S_1(O_1, x_1, y_1)$ are built, which are rigidly connected to the ground and the pinion respectively. The origins of S_f and S_1 coincide with the pinion center, and the pitch line of rack-cutter is tangent to the pitch circle of pinion at point P_t. During the generation, S_t moves with the rack-cutter while S_1 rotates with the pinion. When S_t has a displacement of s, S_1 rotates over an angle of φ_1, both of which are related by equation (5).

$$s = r_1\varphi_1 \tag{5}$$

According to the theory of gearing, the profile of pinion can be obtained by applying coordinate transformation from S_t to S_1, as represented by equation (6).

$$\boldsymbol{R}_1^p(\varphi_1, x_t) = \mathbf{M}_{1t}(\varphi_1)\boldsymbol{R}_t^c(x_t) \tag{6}$$

where $\boldsymbol{R}_1^p(\varphi_1, x_t)$ is the envelope to the family of the rack-cutter surfaces, $\boldsymbol{R}_t^c(x_t)$ is the profile of rack-cutter as illustrated by equations (1) to (4), and $\mathbf{M}_{1t}(\varphi_1)$ is the matrix for coordinate transformation as represented by equation (7).

$$\mathbf{M}_{1t}(\varphi_1) = \begin{bmatrix} \cos\varphi_1 & \sin\varphi_1 & -r_1(\varphi_1\cos\varphi_1 - \sin\varphi_1) \\ -\sin\varphi_1 & \cos\varphi_1 & r_1(\varphi_1\sin\varphi_1 + \cos\varphi_1) \\ 0 & 0 & 1 \end{bmatrix} \tag{7}$$

Given the necessary condition of existence of $\boldsymbol{R}_1^p(\varphi_1, x_t)$, equation (8) should be satisfied.[18]

$$\boldsymbol{N}_t \cdot \boldsymbol{v}_t^{(t1)} = 0 \tag{8}$$

where $\boldsymbol{N}_t$ is the normal to the rack-cutter surface and $\boldsymbol{v}_t^{(t1)}$ is the relative velocity between the rack-cutter and the pinion. Both are represented in S_t.

Meanwhile, $\boldsymbol{N}_t$ and $\boldsymbol{v}_t^{(t1)}$ can be represented as follows

$$\boldsymbol{N}_t = \boldsymbol{T}_t \times \boldsymbol{k}_t = \frac{d\boldsymbol{R}_t^c}{dx_t} \times \boldsymbol{k}_t \tag{9}$$

$$\boldsymbol{v}_t^{(t1)} = \boldsymbol{v}_t^{(t)} - (\boldsymbol{\omega}_t^{(1)} \times \boldsymbol{R}_t^c + \mathrm{E}_t \times \boldsymbol{\omega}_t^{(1)}) \tag{10}$$

where $\boldsymbol{T}_t$ is the tangent to the rack-cutter surface, $\boldsymbol{v}_t^{(t)}$ is the velocity of the rack-cutter, $\boldsymbol{\omega}_t^{(1)}$ is the angular velocity of the pinion and $\boldsymbol{E}_t$ is the position vector drawn from O_t to O_1. They are represented in S_t.

Equations (8) to (10) yield

$$f(\varphi_1, x_t) = \frac{dy_t^c}{dx_t} y_t^c - \frac{dx_t^c}{dx_t}(r_1\varphi_1 - x_t^c) = 0 \tag{11}$$

where $(x_t^{(c)}, y_t^c)$ is the coordinate of the point on the profile of rack-cutter.

Considering equations (6) and (11), the mathematical model of the pinion profile can be obtained, which is defined as the first envelope to generate the internal gear.

The profile of the conjugated involute internal gear

According to the double envelope concept, the profile of the conjugated involute internal gear is regarded as an envelope to the family of the obtained pinion surfaces. Now, the mathematical model of the pinion profile becomes the generating surface and the profile of internal gear is considered as the generated surface.

Another coordinate system $S_2(O_2, x_2, y_2)$ is built to demonstrate the relationship between the pinion and the internal gear during the generation (Figure 2(c)). Here, S_2 is rigidly connected to the internal gear and the origin of S_2 coincides with the gear center. The pitch circles of pinion and internal gear are tangent at point P. The rotation angles of S_1 and S_2, φ_1 and φ_2, are related by equation (12).

$$r_1\varphi_1 = r_2\varphi_2 \tag{12}$$

Then, the profile of internal gear can be obtained by equations (13) and (14).

$$\boldsymbol{R}_2^i(\varphi_1, \varphi_2, x_t) = \mathbf{M}_{21}(\varphi_1, \varphi_2)\boldsymbol{R}_1^p(\varphi_1, x_t) \tag{13}$$

$$\boldsymbol{N}_p \cdot \boldsymbol{v}_1^{(12)} = 0 \tag{14}$$

where $R_2^i(\varphi_1, \varphi_2, x_t)$ is the envelope to the family of the pinion surfaces, $\mathbf{M}_{21}(\varphi_1, \varphi_2)$ is the matrix for coordinate transformation from S_1 to S_2 as represented by equation (15), $\boldsymbol{N}_p$ is the normal to the pinion surface and $\boldsymbol{v}_1^{(12)}$ is the relative velocity between the pinion and the internal gear. $\boldsymbol{N}_p$ and $\boldsymbol{v}_1^{(12)}$ are represented in S_1 by equations (16) and (17), respectively.

$$\mathbf{M}_{21}(\varphi_1, \varphi_2) = \begin{bmatrix} \cos(\varphi_1 - \varphi_2) & -\sin(\varphi_1 - \varphi_2) & (r_2 - r_1)\sin\varphi_2 \\ \sin(\varphi_1 - \varphi_2) & \cos(\varphi_1 - \varphi_2) & (r_2 - r_1)\cos\varphi_2 \\ 0 & 0 & 1 \end{bmatrix} \tag{15}$$

$$\boldsymbol{N}_p = \frac{\partial \boldsymbol{R}_1^p}{\partial \varphi_1} \times \frac{\partial \boldsymbol{R}_1^p}{\partial x_t} \tag{16}$$

$$\boldsymbol{v}_1^{(12)} = (\boldsymbol{\omega}_1^{(1)} - \boldsymbol{\omega}_1^{(2)}) \times \boldsymbol{R}_1^p - \mathrm{E}_1 \times \boldsymbol{\omega}_1^{(2)} \tag{17}$$

where $\boldsymbol{\omega}_1^{(1)}$ is the angular velocity of the pinion, $\boldsymbol{\omega}_1^{(2)}$ is the angular velocity of the internal gear and $\boldsymbol{E}_1$ is the position vector drawn from O_1 to O_2. They are represented in S_1.

Mesh characteristics of the conjugated involute internal gear couple

The principle of internal gear pumps is based on the meshing internal gear couple which causes a change of cavity volumes between gears and chambers. Therefore, the mesh characteristics of gear couple directly decide the flowrate characteristics of the pump. To study the mesh characteristics, the line of action should be derived first, which is the locus of contact points between the surfaces of gear couple.

According to the theory of gearing, the line of action can be represented by equation (18).

$$\boldsymbol{R}_f^l(\varphi_1, x_t) = \mathbf{M}_{f1}(\varphi_1)\boldsymbol{R}_1^p(\varphi_1, x_t) \tag{18}$$

where $\boldsymbol{R}_f^l(\varphi_1, x_t)$ is the line of action and $\mathbf{M}_{f1}(\varphi_1)$ is the matrix for coordinate transformation from S_1 to S_f, as represented by equation (19).

$$\mathbf{M}_{f1}(\varphi_1) = \begin{bmatrix} \cos\varphi_1 & -\sin\varphi_1 & 0 \\ \sin\varphi_1 & \cos\varphi_1 & 0 \\ 0 & 0 & 1 \end{bmatrix} \tag{19}$$

Equations (18) and (19) yield

$$\boldsymbol{R}_f^l(\varphi_1, x_t) = \begin{bmatrix} x_f^l \\ y_f^l \\ 1 \end{bmatrix} = \begin{bmatrix} x_1^p \cos\varphi_1 - y_1^p \sin\varphi_1 \\ x_1^p \sin\varphi_1 + y_1^p \cos\varphi_1 \\ 1 \end{bmatrix} \tag{20}$$

With equation (20), the line of action of the conjugated involute internal gear couple rotating

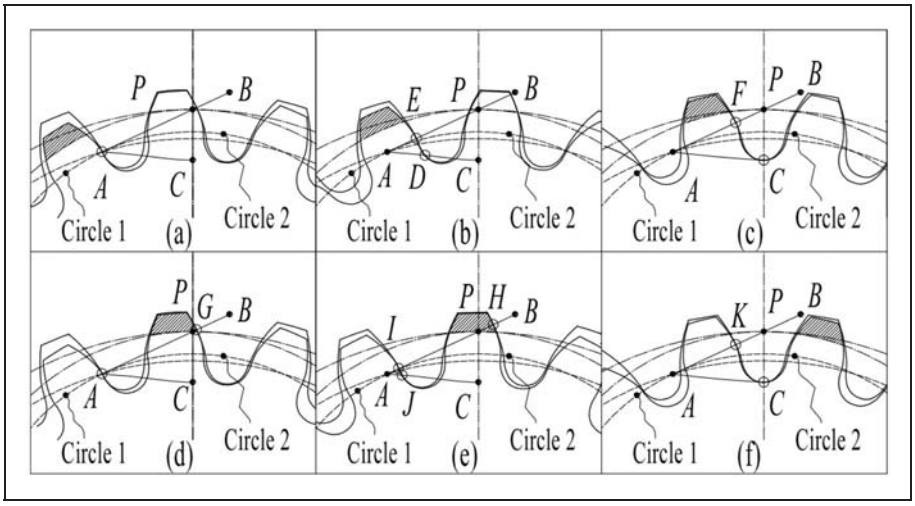

Figure 3. Meshing process of one tooth pair.

clockwise can be obtained, which comprises line AB and curve AC (it seems like a line; Figure 3). Here, line AB is the locus of contact points of the involutes and curve AC is the locus of contact points of the root fillets. Figure 3 demonstrates the meshing process of the gear couple. Here, two circles, Circle 1 and Circle 2, are used to distinguish the involutes and the root fillets in the profiles. To the pinion, the parts of profiles outside Circle 1 are the involutes while those inside Circle 1 are the root fillets, which is the same with Circle 2 to the internal gear. To describe clearly, one tooth pair is taken for the illustration of meshing process, pinion tooth of which is filled with shadow lines. And, the contact points are marked by hollow circles.

Then, the meshing process of one tooth pair can be illustrated as follows:

(a) The target tooth pair comes into mesh at point A.
(b) At this moment, the tooth pair meshes at points D and E simultaneously. As gears continue rotating, point D moves along curve AC while point E along line AB.
(c) The root fillets meshes at point C, the end of curve AC, which indicates they're going to end meshing.
(d) The second tooth pair starts meshing and there are two contact points on line AB, points A and G.
(e) Similarly, the second tooth pair have two contact points, points I and J. Meanwhile, the first tooth pair is still meshing at point H.
(f) After the contact point of the first tooth pair passed point B, the end of line AB, there's only the second tooth pair left meshing.

As mentioned above, besides the involutes, the root fillets also participate into meshing in the conjugated involute internal gear couple, which makes it have more contact points than the none-conjugated one. It's easy to understand more contact points will make the gears transmit more smoothly, which is helpful for the pump to obtain a steady fluid delivery. Also, it will make the meshing teeth suffering from fewer loads and consequently increase the lifetime of the gears and the pump.

Flowrate characteristics of the conjugated involute internal gear couple

It is known gear pumps depend on the mesh movement of gear couple to deliver fluid. Clearly, the mesh movement is periodic and so is the corresponding fluid delivery. Therefore, according to the mesh characteristics represented in the previous section, the fluid delivery process of one tooth pair is employed for illustration of the flowrate characteristics of the pump (Figure 4). Here, there is backlash between the meshing teeth and no relief groove in the pump. To have a clear illustration, only the contact points associated with fluid delivery are marked by hollow circles.

Then, the fluid delivery process of one tooth pair can be illustrated as follows:

(a) As the target tooth pair starts meshing from point A, the chamber between the teeth becomes smaller, which makes the fluid inside the chamber squeezed into the discharge chamber. This is the beginning of the fluid delivery process by the tooth pair.
(b) Though there are involutes and root fillets meshing simultaneously, only the parts of involutes above point D contribute to the fluid delivery.
(c) When the second tooth pair starts delivering, the passage of fluid delivery to the outlet for the target tooth pair is blocked. By now, the first tooth pair has finished delivering. Meanwhile, the fluid enclosed between points A and E is isolated from the discharge chamber and the suction

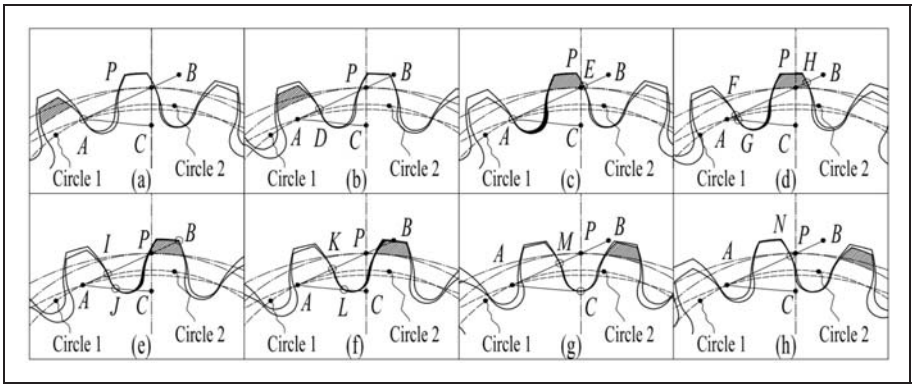

Figure 4. Fluid delivery process of one tooth pair.

chamber, which is known as 'trapped fluid' and filled with black.

(d) The trapped fluid is divided into two parts by point G, which is located on the root fillets.

(e) The target tooth pair meshes at point B and will end meshing at the next moment. Then, the part of trapped fluid enclosed between points J and B will be connected to the suction chamber, which makes this part of trapped fluid eliminated.

(f) The left part of trapped fluid exists in the volume enclosed between points K and L.

(g) The root fillets of the second tooth pair meshes at point C, the end of the root fillets. The last part of trapped fluid will be connected to the suction chamber at the next moment, which indicates the trapped fluid will disappear.

(h) No trapped fluid exists while the second tooth pair is remaining fluid delivery.

Clearly, one tooth pair is not always delivering fluid during the meshing process. The effective fluid delivery only occurs in the process from Figure 4(a) to (c) while the remaining process from Figure 4(c) to (g) presents the process of trapped fluid which results in high pressure pulsation, unbalanced forces and high noise level. Moreover, since the contact point located on the root fillets do not influent the total trapped volume, the process of trapped fluid can be divided into two stages: (i) the process from Figure 4(c) to (e) and (ii) the process from Figure 4(e) to (g). In the first stage, the trapped volume is enclosed by two contact points both located on the involutes. In the second stage, the trapped volume is enclosed by two contact points located on the involutes and the root fillets, respectively. With these divisions, the acting time of effective delivery and trapped fluid can be decided. Then, it is possible to calculate the flowrate characteristics of the pumps, such as displacement, flowrate pulsation and volume of trapped fluid.

With the analysis mentioned above, a control volume approach is applied to derive the instantaneous flowrate formula in the following part. Then, some indices, such as displacement, pulsation coefficient and volume of trapped fluid, are calculated to evaluate the flowrate characteristics of the pump. Here, displacement equals the fluid volume delivered by the pump each revolution and is usually used to evaluate the volumetric capacity of the pump. And, pulsation coefficient is used to describe the fluctuation level of the pump flowrate. Besides these two indices, volume of trapped fluid is also an important index to evaluate the performances of gear pumps.[1]

Derivation of the instantaneous flowrate formula

The control volume approach is often used in the derivation of flowrate formula of gear pumps.[3–12] Two control volumes, V_1 and V_2, are built for the pinion and the internal gear, respectively (Figure 5). With the assumptions of incompressible fluid, no fluid leakage and rigid parts of the pump, the discharge volume of fluid, dV, equals the difference between the input volumes, dV_{i1} and dV_{i2}, and the output volumes, dV_{o1} and dV_{o2}, as represented by equation (21).

$$dV = dV_i - dV_o = (dV_{i1} + dV_{i2}) - (dV_{o1} + dV_{o2}) \tag{21}$$

where

$$dV_{i1} = \frac{1}{2} r_{a1}^2 d\theta_1,\ dV_{o1} = \frac{1}{2} r_{f1}^2 d\theta_1,\ dV_{i2} = \frac{1}{2} r_{a2}^2 d\theta_2,$$
$$dV_{o2} = \frac{1}{2} r_{f2}^2 d\theta_2. \tag{22}$$

Here, the axial thickness of the gear is a unit thickness.

Given the fundamental law of gearing, it is known

$$d\theta_2 = \frac{r_1}{r_2} d\theta_1,\ \omega_1 = \frac{d\theta_1}{dt} \tag{23}$$

Equations (21) to (23) yield the instantaneous flowrate formula

$$Q = \frac{dV}{dt} = \frac{1}{2}\left[(r_{a1}^2 - r_{f1}^2) - \frac{r_1}{r_2}(r_{a2}^2 - r_{f2}^2) \right] \omega_1 \tag{24}$$

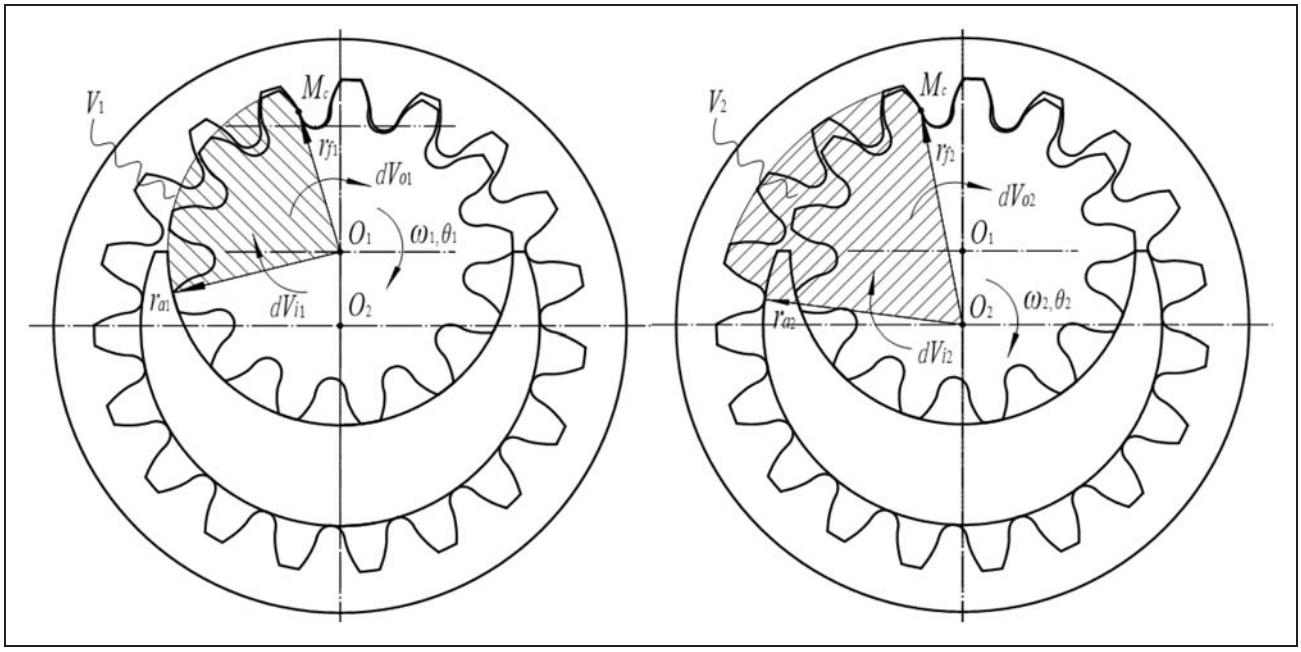

Figure 5. Control volumes for the internal gear pump.

During the delivery process, r_{f1} and r_{f2} can be represented by equations (25) and (26) (Figure 6).

$$r_{f1}^2 = f_{inv}^2 + r_1^2 - 2f_{inv}r_1\cos\alpha \tag{25}$$

$$r_{f2}^2 = f_{inv}^2 + r_2^2 - 2f_{inv}r_2\cos\alpha \tag{26}$$

where f_{inv} is the distance from the contact point M_c to the pitch point P.

Equations (24) to (26) yield

$$Q_{inv}(f_{inv}) = \frac{1}{2}\left[r_{a1}^2 - \frac{r_1}{r_2}r_{a2}^2 - r_1(r_1 - r_2) - \left(1 - \frac{r_1}{r_2}\right)f_{inv}^2\right]\omega_1 \tag{27}$$

It is clear

$$f_{inv} = \sqrt{(x_f^{Mc} - x_f^P)^2 + (y_f^{Mc} - y_f^P)^2},\ (x_f^{Mc}, y_f^{Mc}, 1) \in \boldsymbol{R}_f^{AB}(\varphi_1, x_t) \tag{28}$$

where (x_f^{Mc}, y_f^{Mc}) is the coordinate of point M_c and $\boldsymbol{R}_f^{AB}$ is the position vector of line AB which belongs to $\boldsymbol{R}_f^l$. They are represented in S_f.

Substituting equation (28) into equation (27), the instantaneous flowrate of one tooth pair can be represented by the parameter of the rack-cutter, x_t.

Displacement and pulsation coefficient

The volume delivered by one tooth pair can be given by equation (29).

$$V_Z = \int_{t_{AE}} Q_{inv}(f_{inv})dt \tag{29}$$

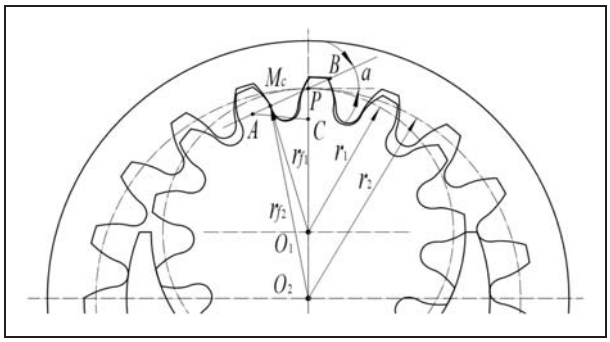

Figure 6. Geometry when gears meshing at point M_c.

where t_{AE} is the lasting time for the contact point moving from point A to point E.

With respect to involutes, a relation is represented by equation (30).

$$\frac{df_{inv}}{dt} = \frac{d(r_{b1}\theta_1)}{dt} = r_{b1}\omega_1 \tag{30}$$

Equations (29) and (30) yield

$$V_Z = \frac{1}{2r_{b1}}\int_{-f_{AP}}^{f_{PE}} [r_{a1}^2 - \frac{r_1}{r_2}r_{a2}^2 - r_1(r_1 - r_2) - (1 - \frac{r_1}{r_2}) \times f_{inv}^2]df_{inv} \tag{31}$$

where f_{PE} and f_{AP} are the lengths of lines PE and AP, respectively. And, the value of f_{inv} is considered as negative before the contact point passes point P.

Then, the displacement of the pump can be obtained by equation (32).

$$q = z_1 V_Z = \frac{z_1}{2r_{b1}} \int_{-f_{AP}}^{f_{PE}} \left[r_{a1}^2 - \frac{r_1}{r_2} r_{a2}^2 - r_1(r_1 - r_2) - \left(1 - \frac{r_1}{r_2}\right) f_{inv}^2 \right] df_{inv} \tag{32}$$

Consequently, the pulsation coefficient, γ, can be defined as follows

$$\gamma = \frac{Q_{\max} - Q_{\min}}{q\omega_1} \tag{33}$$

Volumes of trapped fluid

As mentioned above, the process of trapped fluid includes two stages. In the first stage, the volume of trapped fluid can be obtained by equation (34)

$$\begin{aligned} \Delta V_1 &= \int_{t_{AI}} [Q_{inv}(p_b + f_{inv}) - Q_{inv}(f_{inv})] dt \\ &= \frac{-p_b}{2r_{b1}} \left(1 - \frac{r_1}{r_2}\right) \int_{-f_{AP}}^{-f_{IP}} (p_b + 2f_{inv}) df_{inv} \end{aligned} \tag{34}$$

where t_{AI} is the lasting time for the contact point moving from point A to point I along line AB and f_{IP} is the length of line IP.

Meanwhile, the volume of trapped fluid in the second stage comprises two parts: the volume between the involutes and the volume between the root fillets, as represented by equation (35).

$$\Delta V_2 = \int_{t_{AC}} [Q_{inv}(f_{inv}) + Q_{fil}] dt \tag{35}$$

where t_{AC} is the lasting time for the contact point moving from point A to point C along curve AC, and Q_{fil} is the instantaneous flowrate when contact point moves along the root fillets.

Here, the volume between the involutes can be obtained by equation (36).

$$\int_{t_{AC}} Q_{inv}(f_{inv}) dt = \frac{\omega_1}{2} \int_{-f_{AP}}^{-f_{MP}} \left[r_{a1}^2 - \frac{r_1}{r_2} r_{a2}^2 - r_1(r_1 - r_2) - \left(1 - \frac{r_1}{r_2}\right) f_{inv}^2 \right] df_{inv} \tag{36}$$

Based on equation (24), Q_{fil} can be represented by equation (37).

$$Q_{fil} = Q(x_f^f, y_f^f) = \frac{1}{2} \left[r_{a1}^2 - \frac{r_1}{r_2} r_{a2}^2 - \frac{r_2 - r_1}{r_2} (x_f^f)^2 - (y_f^f - y_f^{O_1})^2 + \frac{r_1}{r_2} (y_f^f - y_f^{O_2})^2 \right] \omega_1 \tag{37}$$

Table 1. Basic design parameters of the gear couple.

Parameter	Value
z_1	13
z_2	19
m	3
α	25°
r_o^*	0.38
h_a^*	0.8
c_n^*	0.3
x	0
ω_1	3000 r/min

where (x_f^f, y_f^f) is the coordinate of the contact point on curve AC, which is represented in S_f.

According to Figure 2(a), equation (2) can be represented with parameter θ:

$$\boldsymbol{R}_t^{bc} = \begin{bmatrix} x_t^{bc} \\ y_t^{bc} \\ z_t^{bc} \end{bmatrix} = \begin{bmatrix} r_o \sin\theta + x_{O_c} - r_1\varphi_1 \\ r_o \cos\theta + y_{O_c} - r_1 \\ 1 \end{bmatrix}, 0 < \theta \leqslant \frac{\pi}{2} - \alpha \tag{38}$$

Equations (6), (18) and (38) yield

$$\begin{cases} x_f^f = r_o \sin\theta + x_{O_c} - r_1\varphi_1 \\ y_f^f = -r_o \cos\theta + y_{O_c} + r_1 \end{cases} \tag{39}$$

Substituting equation (39) into equation (37), Q_{fil} can be represented with parameter θ by equation (40).

$$Q_{fil} = Q_{fil}(\theta) \tag{40}$$

Equations (11) and (39) yield

$$\varphi_1(\theta) = \frac{y_{O_c} \tan\theta + x_{O_c}}{r_1} \tag{41}$$

The derivative of equation (41) yields

$$r_1 d\varphi_1 = \frac{y_{O_c}}{\cos^2\theta} d\theta \tag{42}$$

Then, a relation can be obtained by equation (43).

$$dt = \frac{d\varphi_1}{\omega_1} = \frac{y_{O_c}}{\omega_1 r_1 \cos^2\theta} d\theta \tag{43}$$

Consequently, the volume of trapped fluid between the root fillets can be obtained

$$\int_{t_{AC}} Q_{fil}\, dt = \frac{y_{O_c}}{\omega_1 r_1} \int_{\theta_A}^{\theta_C} \frac{Q_{fil}(\theta)}{\cos^2\theta} d\theta \tag{44}$$

Table 2. Influences of design parameters of gears on flowrate characteristics of the pump.

Design parameter	Value	Displacement	Flowrate pulsation	Trapped volume	Difference of trapped volumes
x	great	↗	V-shaped	↘	↘
	low	↘		↗	↗
z_1	great	↗	↘	↗	↘
	low	↘	↗	↘	↗
z_2	great	insensitive	↗	insensitive	↘
	low		↘		↗
α	great	↗	↘	↘	↘
	low	↘	↗	↗	↗
r_o^*	great	↗	↘	↘	↘
	low	↘	↗	↗	↗

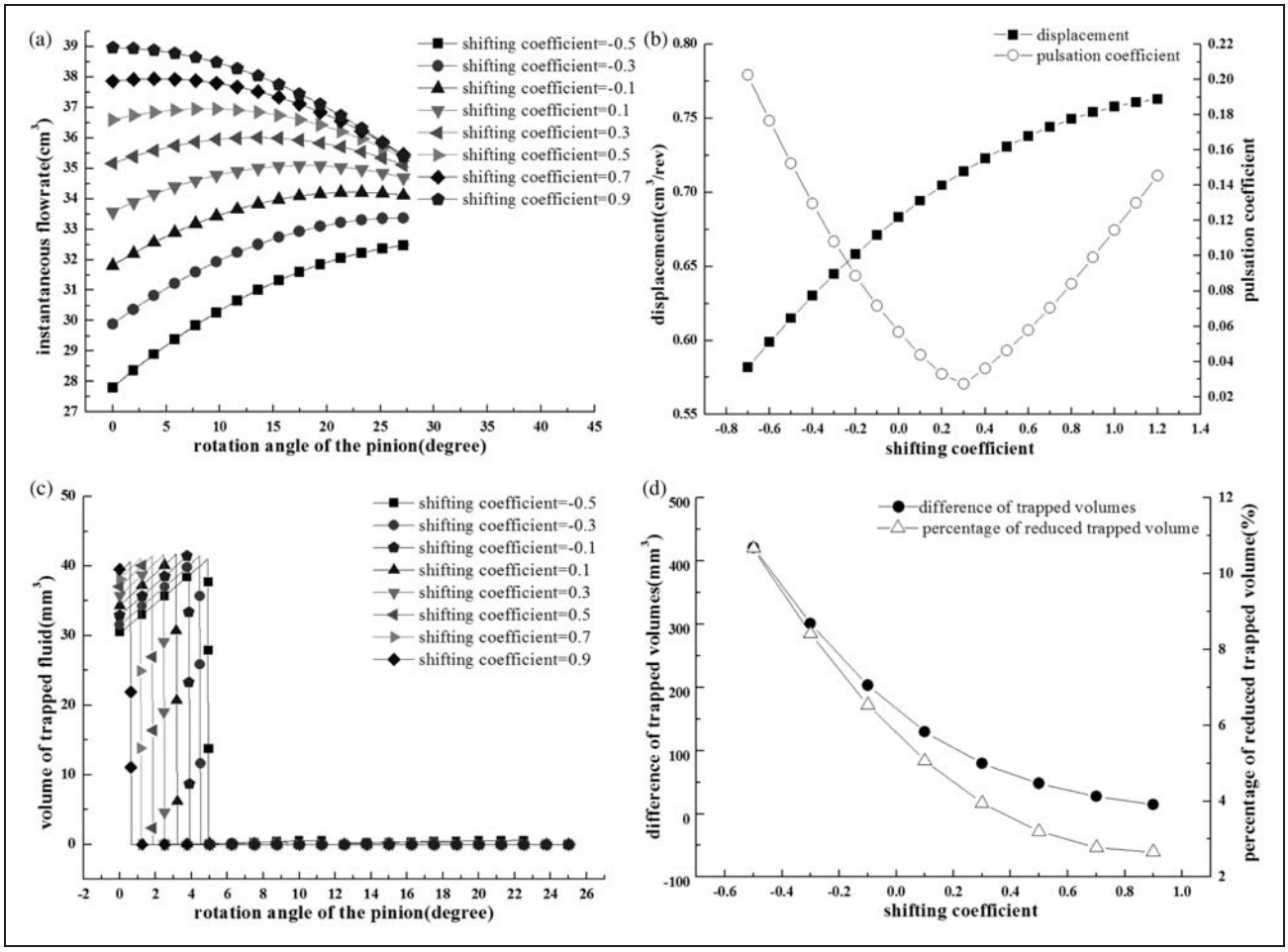

Figure 7. Influences of shifting coefficient: (a) instantaneous flowrate of one tooth pair; (b) displacement and pulsation coefficient; (c) volume of trapped fluid; (d) difference of trapped volumes.

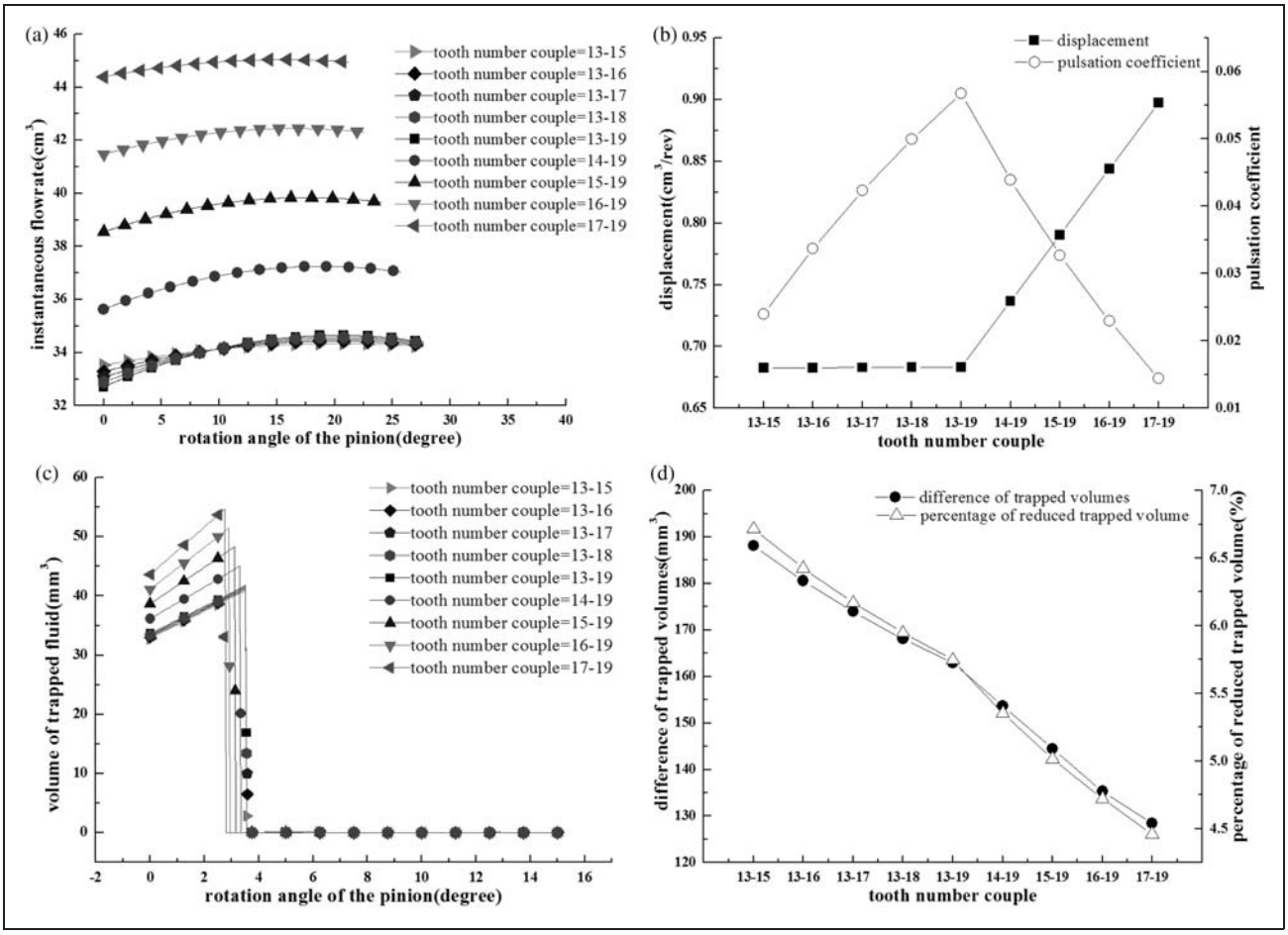

Figure 8. Influences of tooth number: (a) instantaneous flowrate of one tooth pair; (b) displacement and pulsation coefficient; (c) volume of trapped fluid; (d) difference of trapped volumes.

where θ_A and θ_C are the corresponding parameters to points A and C, respectively.

To solve equations (31) to (35), the positions of points E, I, J and M should be determined. With illustrations mentioned above, some relations can be obtained

$$\begin{cases} y_1^E = \tan\alpha x_1^E + r_1 \\ (x_1^E - x_1^A)^2 + (y_1^E - y_1^A)^2 = p_b^2 \end{cases} \tag{45}$$

$$\begin{cases} y_1^I = \tan\alpha x_1^I + r_1 \\ (x_1^I - x_1^B)^2 + (y_1^I - y_1^B)^2 = p_b^2 \end{cases} \tag{46}$$

$$\begin{cases} \angle AO_1I = \varphi_A(\theta_A) - \varphi_I(\theta_J) \\ \cos\angle AO_1I = \frac{\boldsymbol{O_1A}\bullet\boldsymbol{O_1I}}{|\boldsymbol{O_1A}||\boldsymbol{O_1I}|} \\ \boldsymbol{O_1A} = (x_1^A - x_1^{O_1})\boldsymbol{i}_1 + (y_1^A - y_1^{O_1})\boldsymbol{j}_1 \\ \boldsymbol{O_1I} = (x_1^I - x_1^{O_1})\boldsymbol{i}_1 + (y_1^I - y_1^{O_1})\boldsymbol{j}_1 \end{cases} \tag{47}$$

$$\begin{cases} y_1^M = \tan\alpha x_1^M + r_1 \\ \angle AO_1M = \varphi_A(\theta_A) - \varphi_M(\theta_C) \\ \cos\angle AO_1M = \frac{\boldsymbol{O_1A}\bullet\boldsymbol{O_1M}}{|\boldsymbol{O_1A}||\boldsymbol{O_1M}|} \\ \boldsymbol{O_1M} = (x_1^M - x_1^{O_1})\boldsymbol{i}_1 + (y_1^M - y_1^{O_1})\boldsymbol{j}_1 \end{cases} \tag{48}$$

where $(x_1^{O_1}, y_1^{O_1})$, (x_1^A, y_1^A), (x_1^B, y_1^B), (x_1^E, y_1^E), (x_1^I, y_1^I) and (x_1^M, y_1^M) are the coordinates of points O_1, A, B, E, I and M represented in S_1, φ_A, φ_I and φ_M are the positions of the pinion when the gears mesh at points A, I and M, and θ_I and θ_M are the corresponding parameters to points I and M.

Obviously, curve AC is generated by arc bc. And, points A and C are generated by points c and b, respectively. Then (Figure 2(a))

$$\theta_A = \theta_c = \pi/2 - \alpha, \theta_C = \theta_b = 0 \tag{49}$$

Finally, the total volume of trapped fluid can be represented by equation (50).

$$\Delta V = \begin{cases} \Delta V_1, & t_A < t < t_I \\ \Delta V_2, & t_I < t < t_M \end{cases} \tag{50}$$

where t_A, t_I and t_M are the time when the second tooth pair meshes at points A, I and M.

Flowrate characteristics under different design parameters

With a program written by Matlab codes, the functions obtained above can be solved in

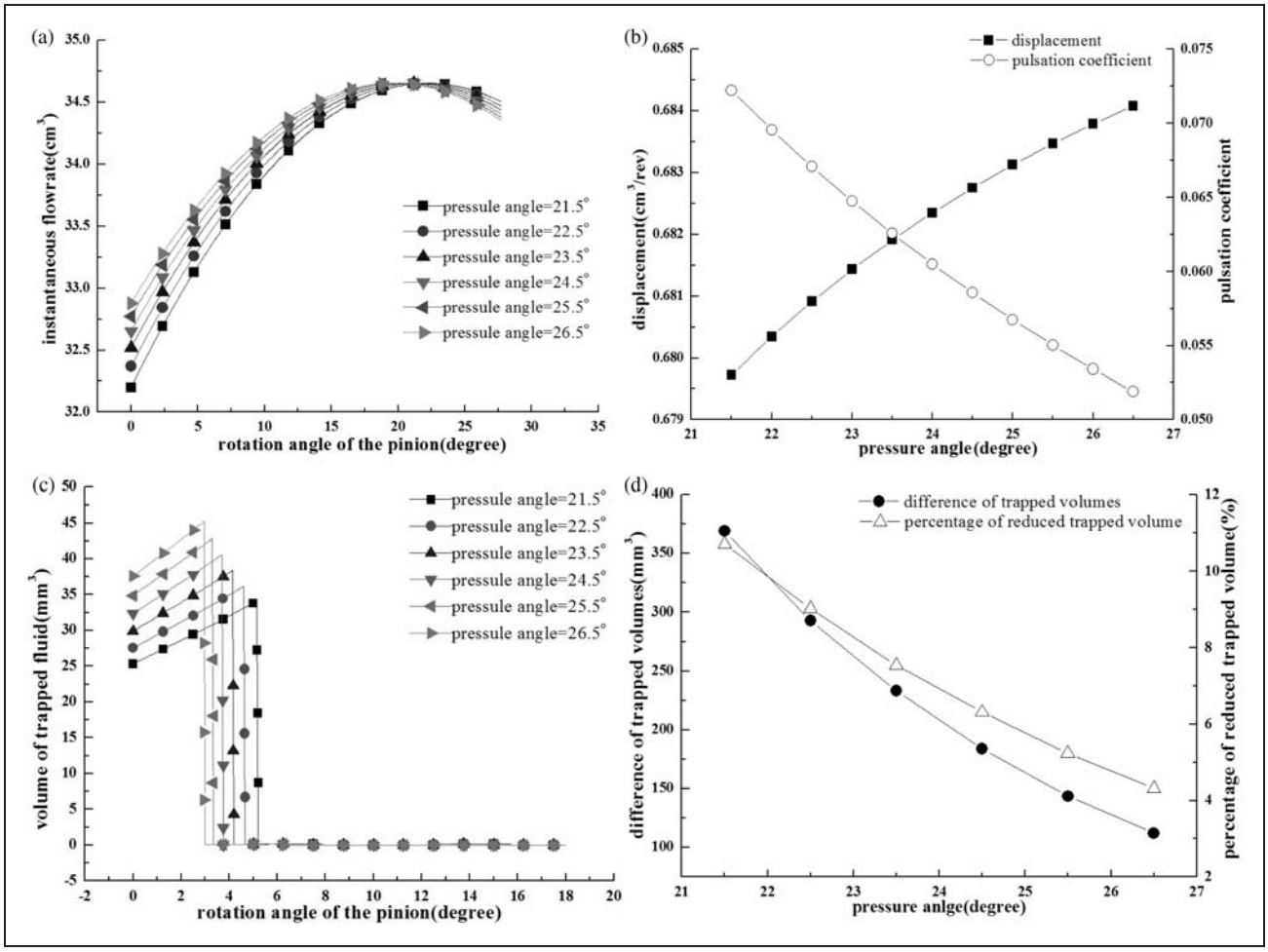

Figure 9. Influences of pressure angle: (a) instantaneous flowrate of one tooth pair; (b) displacement and pulsation coefficient; (c) volume of trapped fluid; (d) difference of trapped volumes.

Matlab environment. Then, influences of design parameters of gears, including shifting coefficient, pressure angle, tooth number and fillet radius, on flowrate characteristics of the pump can be investigated. The basic design parameters of the gear couple are listed in Table 1. Here, possible interferences of teeth are neglected.

Shifting coefficient

In Figure 7(a), as the shifting coefficient gets larger, the flowrate increases with the former point having a larger increment than the latter point. Consequently (Figure 7(b)), the displacement increases with the gradient getting smaller while the pulsation coefficient varies in a V-shaped form. Figure 7(c) reveals the process of trapped fluid is obviously divided into two stages and the volume in the second stage is negligibly small compared to that in the first stage. Besides, a larger shifting coefficient can decrease the total trapped volume, which equals the area surrounded by the curve shown in Figure 7(c), and so does the acting time of trapped fluid. Figure 7(d) shows the difference of trapped volumes between the conventional pump and the conjugated pump. Here, the trapped volume of the conventional pump is obtained referring to the work mentioned in Ichikawa.[13] It is evident the conjugated pump has a smaller trapped volume and the volume difference is reduced with shifting coefficient increasing. With a shifting coefficient of -0.5, the volume difference is about 420.8 mm^3 and about 10.7% of the total trapped volume of the conventional pump.

Tooth number

In Figure 8(a), the flowrate is fairly insensitive to the tooth number of the internal gear. However, increasing the tooth number of the pinion can make the flowrate rise significantly, which also decreases the acting time of fluid delivery. The same happens to the displacement (Figure 8(b)). Only the tooth number of the pinion has a considerable effect on the displacement. Meanwhile, it is of benefit for the flowrate pulsation reduction by increasing the tooth number of the pinion or decreasing the tooth number of the internal gear. In Figure 8(c), it is evident the pinion with a larger tooth number can enlarge the

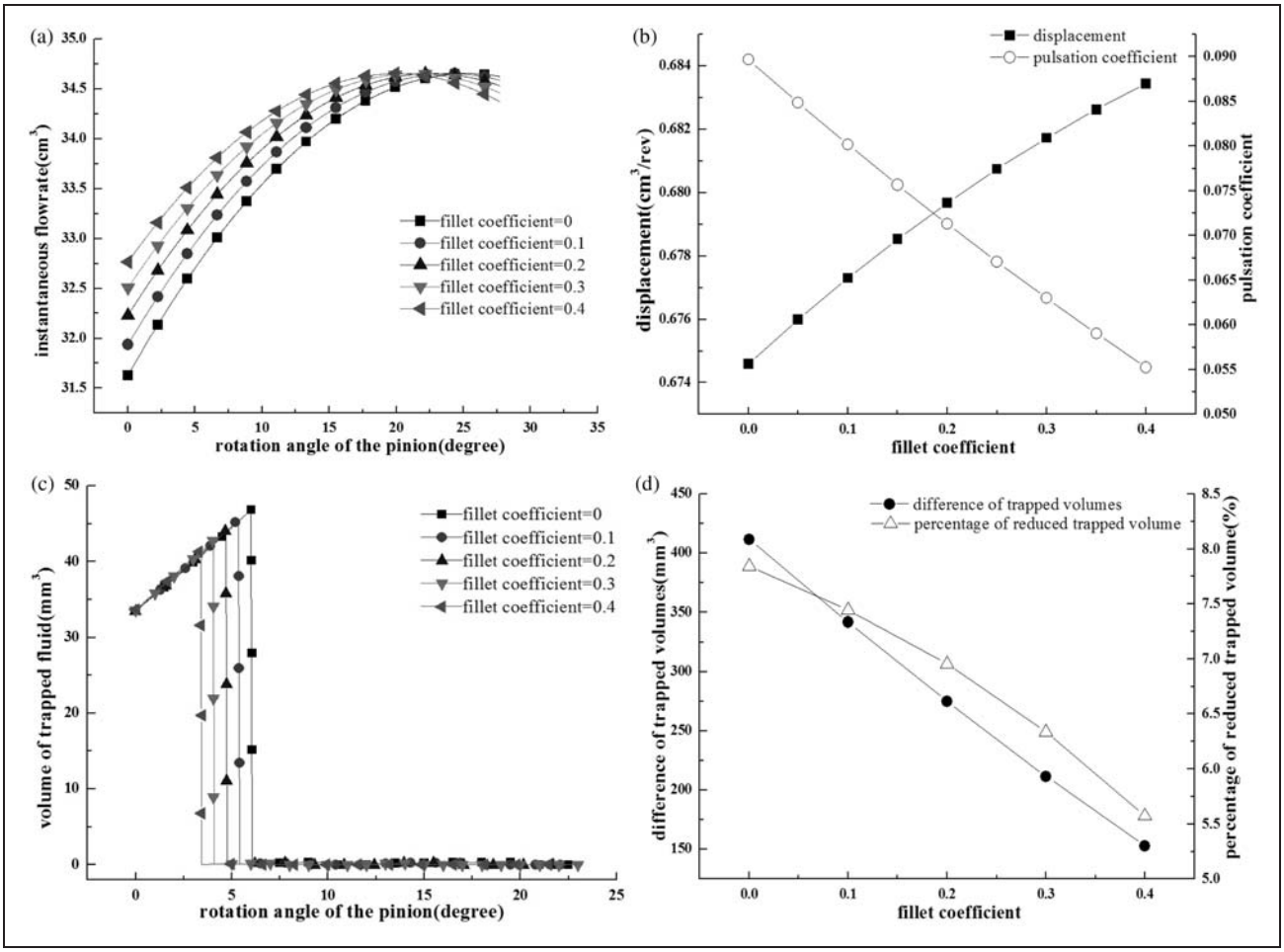

Figure 10. Influences of fillet radius: (a) instantaneous flowrate of one tooth pair; (b) displacement and pulsation coefficient; (c) volume of trapped fluid; (d) difference of trapped volumes.

total trapped volume and decrease the acting time of trapped fluid. However, changing the tooth number of the internal gear almost has no influence on the trapped volume. Figure 8(d) shows the difference of trapped volumes gets smaller with the increasing tooth number of gears. When the tooth number couple is 13–19, pinion versus internal gear, the volume difference is about 162.9 mm^3 and about 5.7% of the total trapped volume of the conventional pump.

Pressure angle

In Figure 9(a) and (b), the larger pressure angle can yield a higher flowrate and consequently lead to a slightly increased displacement with a smaller pulsation coefficient. Also, this can reduce both the total volume and the acting time of trapped fluid (Figure 9(c)). Referring to Figure 9(d), the volume difference gets smaller with pressure angle increasing. With a pressure angle of 21.5°, the volume difference is about 369.0 mm^3 and about 10.7% of the total trapped volume of the conventional pump.

Fillet radius

With the fillet coefficient varying from 0 to 0.4 (Figure 10(a) and (b)), the flowrate gets higher by increasing the fillet radius, which leads to a sight increment of displacement and a reduction of pulsation coefficient. Figure 10(c) illustrates a larger fillet radius can decrease both the total volume and the acting time of trapped fluid. Referring to Figure 10(d), the volume difference gets smaller with fillet radius increasing. With a fillet radius of 0, the volume difference is about 411.7 mm^3 and about 7.8% of the total trapped volume of the conventional pump.

To have a clear summary of these results, Table 2 is presented as follows. Here, the upward arrow means 'increase' while the downward arrow means 'decrease'.

Conclusions

Using the double envelope concept, the mathematical models of the conjugated involute internal gear couple are derived first. Then, some indices of the flowrate

characteristics are obtained based on the control volume approach. Finally, with varying design parameters of gears, investigations into flowrate characteristics of the conjugated pump are carried out. From the analysis and results, some conclusions can be drawn:

1. The conjugated pump has smaller volume of trapped fluid than the conventional pump. Moreover, due to the fact that gears have more contact points, the pump will have a smoother fluid delivery and a longer lifetime than the conventional pump.
2. A larger shifting coefficient is helpful to increase the displacement and reduce the volume of trapped fluid. Moreover, it is possible to choose a proper shifting coefficient to make the flowrate pulsation the least.
3. Increasing the tooth number of the pinion can obtain a greater displacement with a smaller pulsation coefficient. However, this will increase the total volume of trapped fluid.
4. Increasing the tooth number of the internal gear has a slightly influence on the displacement and the total volume of trapped fluid, but aggravates the flowrate pulsation.
5. The displacement can be increased slightly by a larger pressure angle or fillet radius. However, these two methods are effective to reduce both the flowrate pulsation and the volume of trapped fluid.

In summary, the conjugated pump will have a better performance than the conventional pump due to the completely conjugated gear profiles. To design a conjugated pump with good flowrate characteristics, it is feasible to choose a proper shifting coefficient, a larger tooth number of the pinion, a smaller tooth number of the internal gear, a larger pressure angle and a larger fillet radius, under the condition that no tooth interference occurs. Besides, according to the published researches, these methods are also helpful to reduce the pump size, increase load capacity and durability, reduce contact stress and sliding velocity, and increase lubricated film thickness and gear efficiency.[3,17]

Funding

This research was supported by the National Natural Science Foundation of China (Grant No. 51175453).

References

1. Ivantysyn J and Ivantysynova M. *Hydrostatic pumps and motors*. New Delhi: Academia Books International, 2001.
2. Johnston DN and Drew JE. Measurement of positive displacement pump flow ripple and impedance. *Proc IMechE, Part I: J Systems and Control Engineering* 1996; 210: 65–74.
3. Manring ND and Kasaragadda SB. The theoretical flow ripple of an external gear pump. *ASME J Dyn Syst Measure Control* 2003; 125(3): 396–404.
4. Casoli P, Vacca A and Franzoni G. A numerical model for the simulation of external gear pumps, In: *Proceedings of the 6th JFPS Internal Symposium on Fluid Power*, Tsukuba, Japan, 2005, pp.705–710.
5. Huang KJ and Lian WC. Kinematic flowrate characteristics of external spur gear pumps using an exact closed solution. *Mech Mach Theor* 2009; 44: 1121–1131.
6. Huang KJ, Chen CC and Chang YY. Geometric displacement optimization of external helical gear pumps. *Proc I MechE, Part C: J Mechanical Engineering Science* 2009; 223: 2191–2199.
7. Colbourne JR. Gear shape and theoretical flow rate in internal gear pumps. *Trans CSME* 1975; 3(4): 215–223.
8. Bead JE, Yannitell DW and Pennock GR. The effects of the generating pin size and placement on the curvature and displacement of epitrochoidal gerotors. *Mech Mach Theor* 1992; 27(4): 373–389.
9. Gamez-Montero PJ and Codina E. Flow characteristics of a trochoidal-gear pump using bond graphs and experimental measurement. Part 1. *Proc IMechE, Part I: J Mechanical Engineering Science* 2007; 221: 331–346.
10. Gamez-Montero PJ and Codina E. Flow characteristics of a trochoidal-gear pump using bond graphs and experimental measurement. Part 2. *Proc IMechE, Part I: J Mechanical Engineering Science* 2007; 221: 347–363.
11. Mimmi G, Bonandrini G and Rottenbacher C. Theoretical analysis of internal lobe pumps. In: *12th IFToMM World Congress*, Besancon, France, 18–21 June 2009.
12. Bonandrini G, Mimmi G and Rottenbacher C. Theoretical analysis of internal epitrochoidal and hypotrochoidal machines. *Proc IMechE, Part C: J Mechanical Engineering Science* 2009; 223: 1469–1480.
13. Ichikawa T. Characteristics of internal gear pump. *Bull JSME* 1959; 2(5): 35–39.
14. Mimmi G and Pennacchi PE. Involute gear pumps versus lobe pumps: a comparison. *Trans ASME* 1997; 119: 458–465.
15. Litvin FL, Krylov NN and Erikhov ML. Generation of tooth surfaces by two-parameter enveloping. *Mech Mach Theor* 1975; 10: 365–373.
16. Litvin FL and Seol IH. Computerized determination of gear tooth surface as envelope to two parameter family of surfaces. *Comput Meth Appl Mech Eng* 1996; 138: 213–225.
17. Yang SC. Study on an internal gear with asymmetric involute teeth. *Mech Mach Theor* 2007; 42(8): 977–994.
18. Litvin FL. *Gear geometry and applied theory*. Englewood Cliffs, NJ: Prentice-Hall, 1994.

Appendix

Notation

c_n^*	dedendum coefficient
dV	discharge volume of fluid
$dV_{i1,2}$	input volumes for the pinion and the internal gear
$dV_{o1,2}$	output volumes for the pinion and the internal gear

$\boldsymbol{E}_1$ position vector drawn from O_1 to O_2 represented in S_1

$\boldsymbol{E}_t$ position vector drawn from O_t to O_1 represented in S_t

f_{inv} distance from the contact point located on the involutes to the pitch point

h_a^* addendum coefficient

h_a addendum with a value of $h_a^* m$

h_f dedendum with a value of $(h_a^* + c_n^*)m$

m module

$\mathbf{M}_{ij}$ coordinate transformation matrix from coordinate system S_i to coordinate system S_j

$\boldsymbol{N}_p$ normal to the pinion surface

$\boldsymbol{N}_t$ normal to the rack-cutter surface

p tooth thickness with a value of πm

Q_{fil} instantaneous flowrate of the root fillets

Q_{max} maximum of the flowrate

Q_{min} minimum of the flowrate

$r_{1,2}$ pitch radii of the pinion and the internal gear

$r_{a1,2}$ addendum radii of the pinion and the internal gear

r_{b1} base pitch radius of the pinion

$r_{f1,2}$ distances from the contact point to the pinion center and the internal gear center

r_a^* fillet coefficient

r_o fillet radius with a value of $r_o^* m$

$\boldsymbol{R}_1^p$ envelope to the family of the rack-cutter surfaces represented in S_1

$\boldsymbol{R}_2^i$ envelope to the family of the pinion surfaces represented in S_2

$\boldsymbol{R}_f^{AB}$ position vector of line AB represented in S_t

$\boldsymbol{R}_f^l$ line of action represented in S_t

$\boldsymbol{R}_t^c$ profile of the rack-cutter represented in S_t

s displacement of the rack-cutter

$S_{1,2,\,f,t}$ coordinate systems rigidly connected to the pinion, the internal gear, the ground and the rack-cutter respectively

$\boldsymbol{T}_t$ tangent to the rack-cutter surface

$\boldsymbol{v}_1^{(12)}$ relative velocity between the pinion and the internal gear represented in S_1

$\boldsymbol{v}_t^{(t)}$ velocity of the rack-cutter represented in S_t

$\boldsymbol{v}_t^{(t1)}$ relative velocity between the rack-cutter and the pinion represented in S_t

$V_{1,2}$ control volumes for the pinion and the internal gear

x shifting coefficient

x_t parameter of the rack-cutter

$z_{1,2}$ tooth numbers of the pinion and the internal gear

α pressure angle

ΔV total volume of trapped fluid

ΔV_1 volume of trapped fluid between the two contact points both located on the involutes

ΔV_2 volume of trapped fluid between the two contact points located on the involutes and the root fillets respectively

θ parameter of the rack-cutter fillet

$\theta_{1,2}$ rotation angles of the pinion and the internal gear during the delivery process

$\varphi_{1,2}$ angles of the pinion and the internal gear during generation processes

$\omega_{1,2}$ values of the angular velocity of the pinion and the internal gear

$\boldsymbol{\omega}_1^{(1)}$ angular velocity of the pinion represented in S_1

$\boldsymbol{\omega}_1^{(2)}$ angular velocity of the internal gear represented in S_1

$\boldsymbol{\omega}_t^{(1)}$ angular velocity of the pinion represented in S_t